Eur Biophys J (2008) 37:197–204
DOI 10.1007/s00249-007-0216-5

ORIGINAL PAPER

Spider silk softening by water uptake: an AFM study

Arne Schäfer · Thorsten Vehoff · Anja Glišović · Tim Salditt

Received: 9 February 2007 / Revised: 9 August 2007 / Accepted: 24 August 2007 / Published online: 13 September 2007

Abstract We have investigated the mechanical properties of spider dragline fibers of three *Nephila* species under varied relative humidity. Force maps have been collected by atomic force microscopy. The Young's modulus E was derived from the indentation curves of each pixel by the modified Hertz model. An average decrease in E by an order of magnitude was observed upon immersion of the fiber in water. Single fiber stretching experiments were carried out for comparison, and also showed a strong dependence on relative humidity. However, the absolute values of E are significantly higher than those obtained by indentation. The results of this work thus show that the elastic properties of spider silk are highly anisotropic, and that the silk softens significantly for both tensile and compressional strain (indentation) upon water uptake. In addition, the force maps indicate a surface structure on the sub-micron scale.

Keywords Atomic force microscopy · Spider silk · Dragline · Force–strain curves · Young's modulus

Introduction

Spider dragline silk fibers exhibit unusual mechanical properties, such as a combination of tensile strength and extensibility (Vollrath and Knight 2001; Gosline et al. 1999; Fossey and Kaplan 1999, see also Vollrath and Porter (2006) for a recent review. By contrast, most man-made fibers exhibit either high tensile strength and stiffness or low strength and high extensibility. Many experimental studies have been recently undertaken to explain the mechanical properties based upon the macromolecular and supramolecular structural organization of spider silk (Riekel and Vollrath 2000). However, before the structure–property relationship can ultimately be established in a quantitative way, a more detailed knowledge is needed on the mechanical properties and its dependence on environmental parameters. The dependence on temperature and/or humidity is not only important for a fundamental understanding, but will also have practical implications for possible future material applications of spider silk analogues.

In this study we have determined the Young's modulus E from force curves measured by atomic force microscopy (AFM). The force curves have been collected in scanning mode, generating maps of E across the fiber surface. For comparison, single fiber stretching experiments have been made. Thus Young's modulus E along the two symmetry axes, perpendicular and parallel to the fiber can be compared. Both single fiber stretching and AFM measurements have been carried out at different hydration states. The supercontracted state of wet spider silk is well known for its distinctly different stretching curves, which resemble those of synthetic elastomers (Bell et al. 2002; Elices et al. 2005) rather than the curves of higher E and high tenacity (toughness) typical for the dry state.

Atomic force microscopy (Binnig et al. 1986) can be used to monitor biological processes under physiological conditions (Drake et al. 1989) on the cellular (Fritz et al. 1994) and the molecular scale (Radmacher et al. 1994a). In addition to topographical maps of the sample surface, the local mechanical properties of soft samples can be measured by application of very small loading forces (Tao et al. 1992; Radmacher et al. 1995, 1996; Schäfer and

A. Schäfer · T. Vehoff · A. Glišović · T. Salditt (✉)
Institut für Röntgenphysik,
Universität Göttingen, Friedrich-Hund-Platz 1,
37077 Göttingen, Germany
e-mail: tsaldit@gwdg.de

Radmacher 2005; Weisenhorn et al. 1993; Rotsch et al. 1999). By use of the Hertz model for elastic indentations (Hertz 1882; Sneddon 1965) Young's modulus E can be calculated. AFM has been previously used to characterize elastic properties of spider silk by stretching the fiber attached to the AFM tip (Becker et al. 2003; Kesel et al. 2004), but not by indentation. Structural studies of spider silk include Transmission Electron Microscopy (TEM), Scanning Electron Microscopy (SEM) (Putthanarat et al. 2000; Pérez-Rigueiro et al. 2001), as well as X-ray diffraction (Grubb and Jelinski 1997; Riekel et al. 1999) and Transmission X-ray microscopy (TXM) (Glišović and Thieme 2000). Finally, various theoretical models (Zhou and Zhang 2005; Dai et al. 2003) have been proposed to account for the unusual elastic properties.

Materials and methods

Spider silk

The dragline silk (Major Ampullate Silk, MAS) of three different spider species (*Nephila clavipes*, *Nephila senegalensis* and *Nephila madagascariensis*) was investigated for these studies. A variation of forced silking (Work and Emerson 1982) was used to collect the samples. Before silking, the spiders were sedated in the refrigerator for $1\frac{1}{2}$ h at temperatures around 3°C. Afterwards they were fixed on a piece of styrofoam to expose the spinning apparatus. The sedation by cooling prevented injuries of the spider during the fixation. Once they were fully active and mobile again, the spinnerets were stimulated by a brush, and the dragline threads were selected from other silk fibers. Then the two dragline fibers were parted from each other and reeled up separately.

The silk was collected at a speed of about 6–7 cm/s. It has been shown that the silking rate during the forced silking process influences the silk's tensile properties (Magoshi et al. 1985; Cunniff et al. 1994). To allow beta-sheet formation, a certain minimum extrusion rate is required. To create Bombyx mori fibers, for example, this minimum rate is 0.83 cm/s (Magoshi et al. 1985). For higher rates, the strength of the fibers varies slightly with the extrusion rate up to a point, where the rate is too high to let the fiber form properly. The maximum strength of spider silk fibers are obtained at silking rates between 1.5 and 12.2 cm/s (Cunniff et al. 1994), thus in the range of values used in the present work. It is important to note that from optical microscopy as well as from X-ray transmission microscopy, we know that minor ampullate fibers were not adhering to the MAS fibers in our preparation by forced silking. In other words, the procedure was accurate enough to separate the MAS from other fibers, and also to separate twin fibers. The AFM images also did not show any indications for adherence of minor ampullate fibers or other contaminations.

Atomic force microscopy

A commercial AFM (Bioscope, Digital Instruments, Santa Barbara, CA, USA) combined with an Axiomat inverted optical microscope (Zeiss) was used for this study. The optical microscope was used to position the tip above the spider silk. Soft silicon nitride cantilevers (Microlever, Park Scientific, Sunnyvale, CA, USA) with Gold reflex coating on the cantilever back side and a spring constant of about 8 m N/m as well as silicon cantilevers (Olympus Corporation, Tokyo, Japan) with an Aluminium coating and a medium spring constant of about 2 *N/m* were used. The spring constants were estimated from their resonant frequency, 18 and 70 kHz, respectively. The cantilevers had tip semi-angles of 35° and 19°, respectively. The spider silk was fixed with glue (Schneiders-Universalkleber, Schneider, Hambrücken, Germany) on a standard microscope slide that was magnetically attached to the microscope object stage. The fibers were fixed on their ends only. No indication was observed for wetting of the glue on the central parts of the fiber where AFM measurements were performed. The microscope was placed on a granite plate supported by soft rubber bands attached to the ceiling for vibration isolation. In total, 14 spider silk fibers were investigated in a total of 140 measurements.

Stress–strain curves

The force–strain curves were obtained using the LEX 810 linear extensometer from Dia-Stron (Dia-Stron Ltd., Andover, Hampshire, UK). The instrument is equipped with a load cell (force resolution of 0.049 mN) and a DC motor with optical position control (spatial resolution of 1 μm). To fix the fiber on the sample holders with preadjusted length, Dymax 3013 or 3093 UV-curing adhesive (Dymax Europe GmbH, Frankfurt a.M., Germany) was used hardened by a 5 s burst from the COOLLED 2600 UV LED light curing pen (COOLLED Ltd., Whitchurch, Hants, UK). The fiber on the portable sample mount was translated by a vacuum pickup pen into the extensometer. The fiber was extended until breaking, which typically occurred at around 25% of its initial length. The force and the position values were sampled at intervals of 50 ms. The initial length of the fibers was 7.5 mm, the speed of extension was 100 μm/s. Comparable experimental setups and results for force–strain measurements are described in Pèrez-Rigueiro et al. (1998), Shao and Vollrath (1999). The extension rate was chosen such that

the dependence of the mechanical properties on the rate is minimized, while it becomes significant at higher rates, leading to an increase in the tension. Previously reported stretching experiments on spider silk fibers did not specify the relative humidity, or in some cases worked at fixed relative humidity of 60%. For the present study, the extensometer was incorporated in a box, where different levels of relative humidity, could be fixed by different salt reservoirs. Pure water raised the relative humidity inside the chamber to almost 100%, sodium chloride allowed adjustment of about 75%, magnesium nitrate of around 50% and potassium acetate of approximately 25%.The relative humidity and the temperature were measured by a Testo 635 sensor (Testo AG, Lenzkirch, Germany).

To determine the fiber diameters, scanning electron microscopy was performed, using an SEM 515 from Philips operating at 30 kV electron acceleration energy and a Zeiss Supra 35 at 15 kV. The fibers were coated with a thin (14 nm) gold layer. From the analysis of a number of SEM images, values of 2.43±0.43 and 4.0±0.54 μm for *Nephila clavipes* and *Nephila senegalensis* fibers, respectively, were taken as average values for fiber diameters, determined for two species and preparation method described above. The diameter of *Nephila madagascariensis* fibers ranges in between the diameters of *Nephila clavipes* and *Nephila senegalensis*.

Data acquisition and analysis

Elastic or Young's moduli were derived from the force curves (Schäfer and Radmacher 2005). In a force curve the deflection of the AFM cantilever is monitored as a function of its vertical position while approaching the sample (Fig. 1c, d).

From the measured deflection d, the loading force is determined from Hooke's law

$$F = kd. \tag{1}$$

On an infinitely stiff sample, the cantilever deflection d is equal to the piezo movement Δz (Fig. 1a), whereas on a soft sample the deflection is decreased by the elastic indentation (Fig. 1b)

$$d = \Delta z - \delta. \tag{2}$$

δ is the difference of the measured force curve and a calibration curve (force curve on a sample approximating an infinitely stiff sample). In this study we used the software program "Igor" (WaveMetrics, Inc., Lake Oswego, USA) and special Igor marcos written by Domke (Jan 2000; Domke and Rachmacher 1998). Under the assumption of an infinitely stiff tip and a soft, flat sample the Hertz model

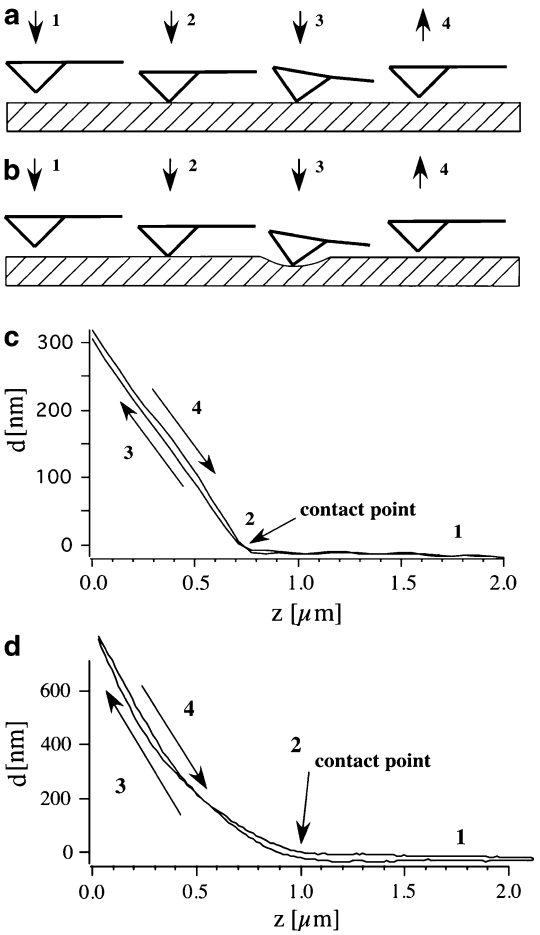

Fig. 1 Schematic of the AFM force measurement by indentation, for the case of **a** stiff and **b** soft surface. The *numbers* in this graph refer to the corresponding sequence in the force curves **c** and **d**: *1* The piezo is approaching to the surface. *2* The AFM tip is in contact with the surface (contact point). *3* The piezo is further moving down, leading to the elastic indentation in the case of a soft surface. *4* The piezo is moving up. **c** Typical force curve of a fiber in the dry state *Nephila senegalensis*. *Z* is the movement of the piezo in the *z* direction and *d* is the cantilever deflection. The *arrows* marks the contact point, the point where the cantilever first comes in contact with the sample surface. The approach and the retraction curves are also indicated by *arrows*. **d** Typical Force curve of a fiber in the wet state (100% humidity). The *slope* of this curve is considerably smaller than that of the stiff sample

predicts the following relation between indentation and loading force. In general, force curves are analyzed as described in Weisenhorn et al. (1993), Rotsch et al. (1999) and (Radmacher 1999), using the Sneddon modification (Sneddon 1965; Johnson 1994) of the Hertz model (Hertz 1882).

$$F = \delta^2 \frac{\pi}{2} \frac{E}{(1-\nu^2)} \tan(\alpha), \tag{3}$$

where E is the elastic or Young's modulus, ν is the Poisson ratio (taken as 0.5 corresponding to an incompressible

material) and α is the opening angle of the cone. We can use Eqs. 1 and 3 to obtain an expression for δ,

$$kd = \delta^2 \frac{\pi}{2} \frac{E}{(1-\nu^2)} \tan(\alpha) \tag{4}$$

$$\delta = \sqrt{\frac{k}{\frac{\pi}{2}\frac{E}{1-\nu^2}\tan(\alpha)}}\sqrt{d} \tag{5}$$

Since δ is not directly detectable by AFM it is replaced by the variables Δz and d.

$$\Delta z = d + \sqrt{\frac{k}{\frac{\pi}{2}\frac{E}{1-\nu^2}\tan(\alpha)}}\sqrt{d} \tag{6}$$

This is the mathematical relation describing the force curve on a soft sample. The zeros of the measured deflection and the sample height are not well defined. To use Eq. 6 for data treatment we need the more general form,

$$|z - z_0| = d - d_0 + \sqrt{\frac{k}{\frac{\pi}{2}\frac{E}{1-\nu^2}\tan(\alpha)}}\sqrt{d - d_0} \tag{7}$$

d_0 and z_0 are the offsets of the sample height and the deflection.

The Young's moduli were calculated from a least squares fit of the Hertz model over all data points inside of the fit area (Radmacher et al. 1996; Jan 2000; Hämmerlin and Hoffmann 1989; Arne 2003). Arrays of typically 32 × 32 force curves were recorded while the tip is raster scanned over the surface (force mapping, force volume mode; Domke and Rachmacher 1998; Radmacher et al. 1994b; Cleveland et al. 1994). Typically, force curves were sampled at 14 curves/s with 64 data points per curve. Data acquisition time for a single force map was about 7 min, this is equivalent to a scan rate of 14 Hz (tip velocity: 55.8 µm/s).

Results

AFM measurements

To check if it is possible to get high-resolution images in the different environments air and water, two-dimensional deflection images in contact-mode of the different spider silks were recorded first. When adding water and immersing the sample and the tip, drifts of the cantilever moved the tip away from the initial contact area. However, for comparison of dry and wet silk, measurements should be performed on the same spot of the sample. For this purpose, the tip was realigned using the optical microscope followed by AFM deflection images. The AFM images showed that it is possible to measure the same sample in both environments and to compare the elasticity results.

In Fig. 2 AFM deflection images of the surface of several spider silk samples are shown. The arrow directions indicate the fiber axis. Each spider silk probe shows a somewhat different surface structure, but most samples show a fibrillar substructure aligned with the fiber axis. No obvious correlation of the structure to spider species was found. In the next step the local modulus E was measured with the AFM. In Fig. 3 two-dimensional force maps are presented for the samples of *Nephila clavipes*. The Young's modulus was calculated off-line after scanning, using Eq. 7. It was not possible to determine E using the soft cantilever in air, because this combination of tip/sample behaves like an infinitely stiff solid surface with no indentation. After switching to the harder cantilever, it was possible to get analyzable data. The experiments typically were started with the samples in air, selecting an 2 × 2µm area on top of the fiber. After recording a few force maps, water was added to sample and E was measured again scanning under water. It was found that for all three kinds of spider silk E decreased significantly after the fibers had come in contact with water.

Figure 3 shows typical 2 × 2µm force maps on top of the *Nephila clavipes* fibers. The measurements in air and

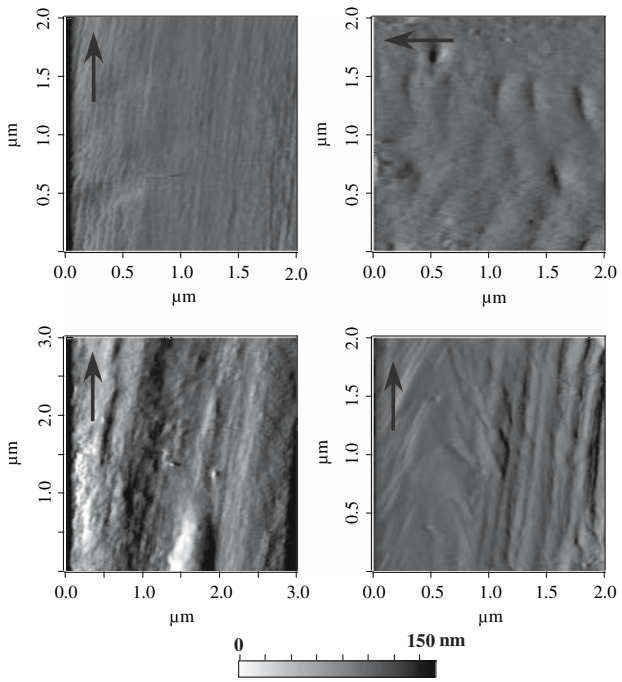

Fig. 2 Typical surface (deflection) images of spider silk fibers. The *two upper images* show fibers of the *Nephila senegalensis*, and the two lower images fibers of the *Nephila clavipes*. The *arrows* mark the direction of the fibers longitudinal axis. Each of the fiber exhibited a different surface structure. Fibers of the same species do not necessarily exhibit the same surface features

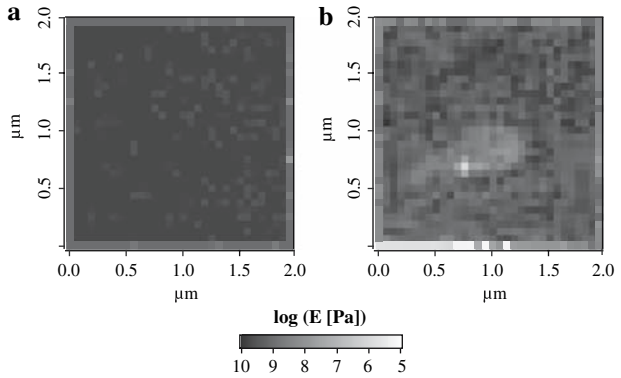

Fig. 3 Elasticity maps of *Nephila clavipes* fibers before (**a**) and after adding water (**b**). The images present only a small area of the top of the spider silk. The elasticity maps show a decrease in E from $\sim 10^{8}.5$–10^{9} to $\sim 10^{7}.5$ –10^{8} Pa after adding water

water were carried out on the same surface area. A decrease in E is clearly observed. The decrease in E is quantified in the histogram shown in Fig. 4. Histograms were generated for each *Nephila clavipes* fibers sample. In air, the maximum of the distribution is at about 10^{9} Pa, while in water it is $10^{8.3}$ Pa. At the same time the width of the distribution increases, probably due to an uneven water uptake of the sample. The errors of E have been determined from the width of the histogram, which quantitatively represent the distribution functions of the measured moduli. The statistical ensemble is already very large for each force maps, because it consists of many independent pixels. In addition a total of about 140 measurements (force maps and deflection images) have been performed on a total of 14 fibers. The error in E is therefore not limited by the statistical ensemble size, and the width of the distribution must reflect an intrinsic property of spider silk. It could be the result of a heterogenous substructure and/or water uptake.

The values tabulated below were calculated by averaging over all points of a force map and all samples of one

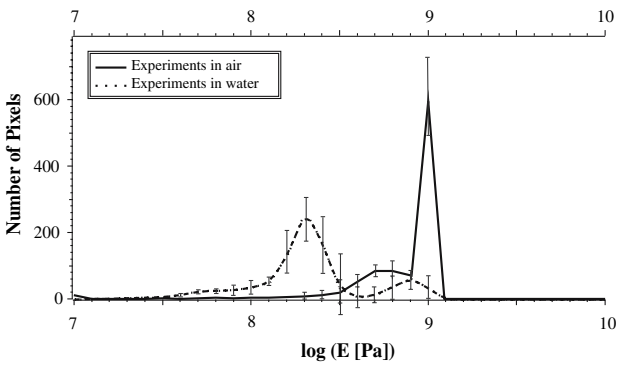

Fig. 4 Histogram of the logarithm of E. Calculated from the images a and b in Fig. 3 representing elasticity data from the top of *Nephila clavipes* fibers

Table 1 Effect of water on the elastic modulus

Species	log (E [Pa]) in air	log (E [Pa]) in water
N. senegalensis	7.1 ± 0.1	6.4 ± 0.4
N. madagascariensis	8.0 ± 0.05	6.7 ± 0.4
N. clavipes	8.8 ± 0.1	8.4 ± 0.3

species. The experiments show that the modulus for all fibers is reduced in water. Quantitatively, the decrease is different for fibers of different spider species. The average maxima and the standard deviation are shown in Table 1.

Stress–strain curves

The indentation results of E by AFM can be compared to the E values determined from stretching (stress–strain) curves. Beforehand, it is clear that the two different elasticity experiments probe a very different sample response to external forces. Firstly, the AFM probes the distortion upon indentation (local compression), while the stretching experiment probes the force upon extension. Secondly, the AFM probes elasticity perpendicular to the fiber, while stretching probes elasticity along the fiber. Finally, the AFM probes the elastic response at a frequency of 14 Hz (tip velocity: 55.8 µm/s), while the stretching rate of 100µm/s corresponds to a frequency, which is slower by a factor of about 2. Figure 5 shows the typical shape of the stress–strain curve for the dry (25% humidity) and the wet (nominally 75% humidity) state, respectively. For humidity control, the extensometer was incorporated in an environmental chamber, where different levels of RH could be set. For relative humidities of about 25% we used a steady flow of nitrogen through the chamber, nominally 75% were obtained by a water bath saturated with sodium chloride (NaCl) inside the chamber. The relative humidity and the temperature were measured by a testo 635 sensor (Testo AG, Lenzkirch, Germany). Note that for a saturated NaCl solution one would expect 75% as the tabulated value for a closed chamber in thermal equilibrium. However this value was not reached in the chamber used. The measured value was 70%.

Upon hydration, the plateau following the linear regime slowly increases, while the linear regime itself decreases, until an elastomeric curve shape is observed for silk completely immersed in water, see also Gosline et al. (1994). This change of curve shape is accompanied by a significant decrease in the elastic modulus, inferred from the initial linear regime. In Fig. 5, the solid lines indicate the regime of linear elastic response, where the modulus was determined from a linear fit (solid lines). As an

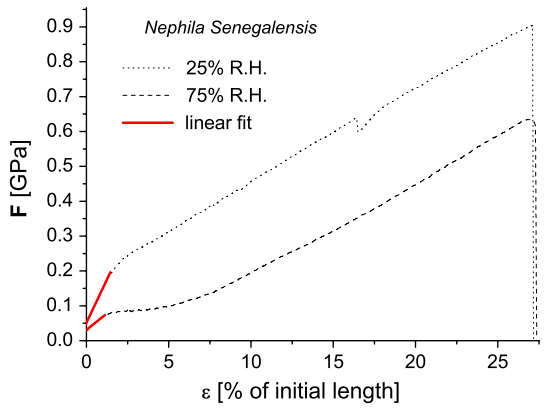

Fig. 5 Stress–strain curves of single *Nephila Senegalensis* spider silk fibers at 25 and 75% humidity. F is the loading force and ε the strain of the fibers. The elastic modulus decreases from 9.9 GPa at 25% humidity to 3.5 GPa at 75% humidity. The linear regression fits are shown as *solid lines*

example, the two least-square linear regression fits shown in Fig. 5 correspond to 9.9 and 3.5 GPa, respectively, for the two hydration states of the sample.

Discussion

The experiments show a significant decrease in Young's modulus E after adding water to spider silk samples. The effect was observed in three different *Nephila* species and on all locations on the surface of the fiber probed by the AFM tip. The spatial distribution of E values and the respective decrease is inhomogeneous, possibly due to a spatially uneven water uptake. The elasticity map shows a tessellated structure (see Fig. 3b).

To explain the results, we assume that the water permeates into the fibers and will be incorporated in the amorphous matrix (Riekel and Vollrath 2000). Thereby the amino acid chains are hydrated by the water molecules. This hydration may interfere with the hydrogen bonding between the chains (Bell et al. 2002; Vollrath and Edmonds 1989), leading to a higher orientational mobility of the chains. This increasing mobility and reduced intramolecular bonds may give an molecular explanation for the macroscopic decrease in the fiber's Young's modulus. Note that the increase in mobility with hydration has been evidenced by solid-state NMR (Kishore et al. 2002). It also explains the tessellated structure, because the concentration of water in the fiber is likely to be non-uniform, because the silk proteins (spidroin 1 and spidroin 2) have hydrophilic and hydrophobic domains (Xu and Lewis 1990; Hinman and Lewis 1992). The stress–strain curves show a similar decrease in E upon hydration. Although the fibers were not completely wetted, the elastic modulus decreased with higher relative humidity. Data of complete wetting (with fibers of different species) are reported in Gosline et al. (1994).

It must be pointed out that the values of E obtained in the stretching experiments are strikingly higher than those inferred from indentation. The loading force of the two different experiments (the AFM experiment and the stress–strain experiment) is of the same magnitude $\sim 10^8$ N/m^2. The loading rate in μ/s of the AFM force curves is two times higher than the stretching rate. The rate of relative extension, however, is more than three orders of magnitude slower by the force–strain experiment compared to that of the AFM experiment, ruling out viscoelastic effects as an explanation for the difference. If viscoelastic effects were important in this range, they would lead to higher not lower AFM values. Hence the most obvious explanation is the anisotropic nature of silk fibers. Already the fiber symmetry of the anisotropic β-sheet crystal orientation indicates that silk fibers cannot be modeled as an elastically uniform body. Based on fiber symmetry we can write down the elasticity equations for the tetragonal crystal system as a function of vertical and lateral strain (Landau and Lifschitz 1965), with the additional assumption of symmetric lateral strain in the case of the stretching experiments $u_{xx} = u_{yy}$, as

$$\sigma_{xx} = \lambda_{xxxx}u_{xx} + \lambda_{xxyy}u_{yy} + \lambda_{xxzz}u_{zz}$$

$$\sigma_{zz} = \lambda_{zzzz}u_{zz} + 2\lambda_{xxzz}u_{xx}$$

σ is the elastic stress, taken along the z-direction for the force–strain experiment and in x-direction for the AFM experiment, λ are the stiffness coefficients and u the strain tensor. It is clear from the number of independent coefficients, that vertical stretching and lateral compression must by no means give the same (effective) elastic modulus, but are completely decoupled. However, the variation of the effective E for both symmetry axes is surprisingly large, and difficult to envision for continuous elastic bodies. Such behavior is typically found in structured bodies. Taking a macroscopic example, Manila rope is an object with large E along the fiber axis, but easy to impress or indent. We can speculate whether similar effects apply on the mesoscopic scale, e.g. associated to micro-fibrils, but to date do not have any structural evidence for this. In fact, X-ray transmission images point to a rather homogenous structure on the length scale below the fiber diameter. Alternatively, we must critically discuss the validity of the absolute values obtained from the AFM indentation experiments. The validity of the Hertz model can clearly be debated, and the analysis of the force curves can also run into problems, in particular if the shape of the curves does not conform to the model. This is particularly problematic for the dry samples, where the functional form of the force curves becomes rather linear. Therefore, the

absolute value for E must be regarded with caution. However, the softening with water uptake is not affected by these complications, and neither is the presence or absence of structures in the force maps.

Thus, the results clearly show that water uptake causes a significant transition in spider silk fibers of the investigated *Nephila* species. It is evident that water has a great influence on the elastic properties of the spider silk fibers. The change from stiff to compliant tensile properties has been recently associated with a transition from a glassy to a rubbery state of silk, depending both on temperature and relative humidity (Plaza et al. 2006). Here, the effect of hydration on elastic properties has been investigated for the first time along the two main symmetry axes of the spider silk fibers, parallel and perpendicular to the fiber axis.

References

Arne Schäfer (2003) Untersuchung mechanischer Eigenschaften von Zellen mit dem Kraftmikroskop - Einfluss von Myosin II. Disseration. Georg-August-Universität Göttingen

Becker N, Oroudjev E, Mutz S, Cleveland JP, Hansma PK, Hayashi CY, Makarov DE, Hannma HG (2003) Molecular nanosprings in spider capture-silk threads. Nat Mater 2:278–283

Bell FI, McEwen IJ, Viney C (2002) Fibre science: supercontraction stress in wet spider dragline. Nature 416:37

Binnig G, Quate CF, Gerber C (1986) Atomic force microscope. Phys Rev Lett 56:930–933

Cleveland JP, Radmacher M, Hansma PK (1994) NATO advanced research workshop AIP. Schluchsee, Germany, pp 543–549

Cunniff PM, Fossey SA, Auerbach MA, Song JW (1994) Mechanical properties of major ampullate gland filk fibers extracted from *Nephilia clavipes* spiders. Silk polymers: materials science and biotechnology, Chap. 21

Dai L, Zhang Y, Ou-Yang Z (2003) Elastic theory of single spider silk protein molecule. Thin Solid Films 438–439:382–385

Domke J (2000) Mikromechanische Eigenschaften dünner Polymerfilme und lebender Zellen. Dissertation. Ludwig-Maximilian-Universität München

Domke J, Rachmacher M (1998) Measuring the elastic properties of thin polymer films with the atomic force microscope. Langmuir 14:3320–3325

Drake B, Prater CB, Weisenhorn AL, Gould SAC, Albrecht TR, Quate CF, Cannell DS, Hansma HG, Hansma PK (1989) Imaging crystals, polymers and biological processes in water with AFM. Science 243:1586–1589

Elices M, Pérez-Rigueiro J, Plaza GR, Guinea GV (2005) Finding inspiration in Argiope trifasciata spider silo fibers. J Mater 57:60–66

Fossey SA, Kaplan DL (1999) Silk protein. In: Polymer data handbook. Oxford University Press, Oxford

Fritz M, Radmacher M, Gaub HE (1994) Granula motion and membrane spreading during activation of human platelets imaged by AFM. Biophys J 66:1328–1334

Glišović A, Thieme J, Guttmann P, Salditt T (2007) Transmission X-ray microscopy of spider dragline silk. Int J Biol Macromol 40:87–95

Gosline JM, Pollak CC, Guerette PA, Cheng A, DeMont ME, Denny MW (1994) Elastomeric network models for the frame and viscid silks from the orb web of the spider *Araneus diadematus*. Silk polymers: materials science and biotechnology. In: Kaplan D, Adams WW, Farmer B, Viney C (eds). American Chemical Society, Washington, DC, pp 328–341

Gosline JM, Guerette PA, Ortlepp CS, Savage KN (1999) The mechanical design of spider silks: from Fibroin sequence to mechanical function. J Exp Biol 202:3295–3303

Grubb DT, Jelinski LW (1997) Small angle X-ray scattering of spider dragline silk. Marcomolecules 30:2860–2867

Hämmerlin G, Hoffmann K-H (1989) Numerische Mathematik. Springer, Berlin

Hertz H (1882) Über die Berührung fester elastischer Körper. Reine Angew Mathematik 92:156–171

Hinman MB, Lewis RV (1992) Isolation of a clone encoding a second dragline silk fibroin, *Nephila Clavipes* dragline silk is a two protein fiber. J Biol Chem 267:19320–19324

Johnson KL (1994) Contact mechanics. Cambridge University Press, Cambridge

Kesel AB, Martin A, Seidl T (2004) Getting a grip on spider attachment: an AFM approach to microstructure adhesion in arthropods. Smart Mater Struct 13:512–518

Kishore AI, Herberstein ME, Craig CL, Separovic F (2002) Solid-state NMR relaxation studies of Australian spider silks. Biopolymers 61:287–297

Landau LD, Lifschitz EM (1965) Band 7 Elastizitätstheorie. Lehrbuch der theoretischen Physik. Verlag Harri Deutsch, Frankfurt am Main

Magoshi J, Magoshi Y, Nakamura S (1985) Physical properties and structure of silk. Polym Comm 26:309–311

Pèrez-Rigueiro J, Viney C, Llorca J, Elices M (1998) Silkworm silk as an engineering material. J Appl Polym Sci 70:2439–2447

Pérez-Rigueiro J, Elices M, Llorca M, Viney C (2001) Tensile properties of Argiope trifasciata drag line silk obtained from the spider's web. J Appl Polym Sci 82:2245–2251

Plaza GR, Guinea GV, Pérez-Rigueiro J, Elices M (2006) Thermo-hygro-mechanical behaviour of spider dragline silk: glassy and rubbery states. J Polym Sci 44:994–999

Putthanarat S, Stribeck N, Fossey SA, Eby RK, Adams WW (2000) Investigation of the nanofibrils of silk fibers. Polymer 41:7735–7747

Radmacher M (1999) Single molecus feel the force. Phys World 12(9):33–37

Radmacher M, Fritz M, Hansma HG, Hansma PK (1994a) Direct observation of enzyme activity with the atomic force microscope. Science 265:1577–1579

Radmacher M, Cleveland JP, Fitz M, Hansma HG, Hansma PK (1994b) Mapping interaction forces with the atomic force microscope. Biophys J 66:2159–2165

Radmacher M, Fritz M, Hansma PK (1995) Imaging soft samples with the atomic force microscope: gelatin in water and propanol. Biophys J 69:264–270

Radmacher M, Fritz M, Kacher MK, Cleveland JP, Hansma PK (1996) Measuring the elastic properties of human platelets with the atomic force microscope. Biophys J 70:556–567

Riekel C, Vollrath F (2001). Spider silk fibre extrusion: combined wide- and small-angle X-ray microdiffraction experiments. Int J Biol Macromol 29:203–210

Riekel C, Müller M, Vollrath F (1999) In situ X-ray diffraction during forced silking of spider silk. Macromolecules 32:4464–4466

Rotsch C, Jacobson K, Radmacher M (1999) Dimensional and mechanical dynamics of active and stable edges in motile fibroblasts investigated by atomic force microscopy. Proc Natl Acad Sci USA 96:921–926

Schäfer A, Radmacher M (2005) Influence of myosin II activity on stiffness of fibroblast cells. Acta Biomaterialia 1:273–280

Shao Z, Vollrath F (1999) The effect of solvents on the contraction and mechanical properties of spider silk. Polymer 40:1799–1806

Sneddon IN (1965) The relation between load and penetration in the axisymmetric Boussinesq problem for a punch of arbitrary profile. Int J Eng Sci 3:47–57

Tao NJ, Lindsay SM, Lees S (1992) Measuring the microelastic properties of biological material. Biophys J 63:1165–1169

Vollrath F, Edmonds DT (1989) Modulation of the mechanical properties of spider silk by coating with water. Nature 340:305–307

Vollrath F, Knight DP (2001) Liquid crystalline spinning of spider silk. Nature 410:541–548

Vollrath F, Porter D (2006) Spider silk as archetypal protein elastomer. Soft Matter 2:377–385

Weisenhorn AL, Khorsandi M, Kasas S, Gotozos V, Celio MR, Butt HJ (1993) Deformation and height anomaly of soft surfaces studied with the AFM. Nanotechnology 4:106–113

Work RW, Emerson PD (1982) An apparatus and technique for the forcible silking of spiders. J Arachnol 10:1–10

Xu M, Lewis RV (1990) Structure of a protein superfiber: spider dragline silk. Proc Natl Acad Sci 87:7120–7124

Zhou H, Zhang Y (2005) Hierarchical chain model of spider capture silk elasticity. Phys Rev Lett 94:028104-1–028104-4